arXiv:1603.04731v3 [hep-ph] 5 Nov 2016

Empirical Parameterization of Nucleon-Nucleon Elastic Scattering Amplitude at High Beam Momenta for Glauber Calculations and Monte Carlo Simulations

V. Uzhinsky[1], A. Galoyan[2], Q. Hu[3,4], J. Ritman[4,5,6], H. Xu[4]

A parameterization of the nucleon-nucleon elastic scattering amplitude is needed for future experiments with nucleon and nuclear beams in the beam momentum range of 2 – 50 GeV/c/nucleon. There are many parameterizations of the amplitude at $P_{lab} > 25$–50 GeV/c, and at $P_{lab} \leq 5$ GeV/c. Our paper is aimed to cover the range between 5 – 50 GeV/c.

The amplitude is used in Glauber calculations of various cross sections and Monte Carlo simulations of nucleon-nucleon scatterings. Usually, the differential nucleon-nucleon elastic scattering cross sections are described by an exponential expression. Corresponding experimental data on *pp* interactions at $|t| > 0.005$ $(\mathrm{GeV/c})^2$ and $|t| \leq 0.125$ $(\mathrm{GeV/c})^2$ have been fit. We propose formulae to approximate the beam momentum dependence of these parameters in the momentum range considered. The same was done for *np* interactions at $|t| \leq 0.5$ $(\mathrm{GeV/c})^2$. Expressions for the momentum dependence of the total and elastic cross sections, and the ratio of real to imaginary parts of the amplitude at zero momentum transfer are also given for *pp* and *np* collisions. These results are sufficient for a first approximation of the Glauber calculations. For more exact calculations we fit the data at $|t| > 0.005$ $(\mathrm{GeV/c})^2$ without restrictions on the maximum value of $|t|$ using an expression based on two coherent exponential. The parameters of the fits are found for the beam momentum range 2 – 50 GeV/c.

Introduction

Parameterizations of nucleon-nucleon elastic scattering amplitude are widely used in many Glauber calculations, for example, for studies of the structure of exotic nuclei and the neutron skin of nuclei [1] – [17], calculations of differential and total reaction cross sections for hadron-nucleus and nucleus-nucleus interactions [18, 19], experimental research of high energy nucleus-nucleus collisions at various impact parameters [20, 21], etc. Considering a nucleon-nucleus interaction, it is sufficient for a first approximation to know the amplitude at zero scattering angle, where the nucleon-nucleon interaction radius (~ 1 fm) is smaller than the nuclear size. The amplitude is connected with the total cross section and the ratio of real to imaginary parts of the amplitude at small momentum transfer. Thus, the parameterizations allow one to extract the total cross section, and the ration for calculations of properties of hadron-nucleus scatterings.

For estimations of geometrical properties of inelastic hadron-nucleus and nucleus-nucleus reactions, a so-called "inelastic nucleon-nucleon interaction profile" is used. The profile is also connected with the amplitude. Very often simplified parameterizations are used for this profile. However, modern experiments in high energy physics and planned experiments with exotic nuclei require very accurate calculations. Thus, a good knowledge of the amplitude is very important for various applications.

A standard parameterization of the spin averaged nucleon-nucleon elastic scattering amplitude is:

$$d\sigma/dt = \pi|F(t)|^2 = |A|^2 e^{Bt}, \tag{1}$$

$$\sigma^{tot} = 4\pi Im(F(0)), \tag{2}$$

$$A = \frac{\sigma^{tot}}{4\sqrt{\pi}}(i+\rho), \tag{3}$$

$$\rho = Re(F(0))/Im(F(0)).$$

[1]Laboratory of Information Technologies, JINR, Dubna, Russia.
[2]Veksler and Baldin Laboratory of High Energy Physics, JINR, Dubna, Russia.
[3]Key Laboratory of High Precision Nuclear Spectroscopy and Center for Nuclear Matter Science, Institute of Modern Physics, Chinese Academy of Sciences, Lanzhou 730000, China.
[4] Institut für Kernphysik, Forschungszentrum Jülich, Jülich, 52425, Germany.
[5]Ruhr-Universität-Bochum, Bochum, 44780, Germany
[6]JARA-FAME, Jülich, 52425, Germany.

A set of its parameters (A, B, and sometimes σ^{tot} and ρ) at various beam momenta below 3 GeV/c [22] is widely applied in calculations at low and intermediate energies (see also [23]). In principle, the parameters can be obtained by fitting the partial wave analysis results [24] – [30], [31] at momenta below 5 GeV/c as done in [22]. Predictions of the partial wave analysis in a tabulated form are used in the PLUTO event generator [32] and in the Geant4 toolkit [33].

At momenta higher than $\sim$ 20 GeV/c, there are many parameterizations of the momentum dependence of the total nucleon-nucleon cross section and ρ including ones by the Particle Data Group (PDG) [34]. Recently, formulae for values of the slope parameter, B, were presented in [35].

A large set of data on proton-proton differential cross sections, analyzing powers and the double polarization parameter, A_{NN}, at proton beam momenta from 3 GeV/c to 50 GeV/c were analyzed in [36] employing the Regge formalism. ρ, ω, f_2, and a_2 trajectories and single-Pomeron exchange were considered. A complicated form of the reggeon amplitudes prevents its simple application in Glauber calculations.

In Sec. 1, we present fits of differential proton-proton elastic scattering cross sections by Eq. 1 in the momentum range 2 – 50 GeV/c. Approximate formulae for the momentum dependence of the parameters are given. We also check the self-consistency of the fitted A, σ^{tot} and ρ parameters. Here, we use the latest data of COSY [37] to estimate ρ in the momentum range 1.7 – 3.6 GeV/c.

The simple exponential parameterization cannot describe the experimental data at large $|t|$ values, especially at $|t| \geq$1–1.5 (GeV/c)^2, where the slope of the differential cross sections becomes smaller. Thus, integration of Eq. 1 will lead to an underestimation of elastic cross section, σ^{el}, and to an overestimation of the inelastic one. A new expression for the differential cross section is needed.

A very simple and transparent parameterization of the elastic scattering amplitude was proposed in Ref. [38] with an analysis of antiproton-proton data at P_{lab} = 1.11, 1.33, and 1.52 GeV/c. A wider set of the $\bar{p}p$ data was considered in references [39, 40, 41, 42]. An analogous parameterization was independently proposed in [43]. The authors of that paper analyzed only pp experimental data at P_{lab} =12, 14.2, 19.2, 24, 29.7 GeV/c and at $\sqrt{s_{pp}}$ = 53 GeV. However, the reduced χ^2/NDF values and the parameter errors were not given. Various extensions of the parameterization were proposed at higher momenta [44, 45, 46, 47]. Its application to low momentum data is complicated by a restricted range of $|t|$ in many cases. Thus, we simplified the model in Sec. 2 and included in our analysis data from the EDDA Collaboration [48] (E =0.23 – 2.59 GeV, $\theta_{c.m.}$ =30° – 90°). In addition to those data, we added optical points that were calculated using σ^{tot} and ρ. This allowed us to clarify the behaviour of the fit parameters in the momentum range 2.3 – 3.8 GeV/c.

In Sec. 3 we turn to the analysis of np elastic scattering data, and obtain analogous results. A short conclusion is presented at the end of the paper.

1 Standard parameterization of pp elastic scattering data

The amplitude of elastic proton-proton scattering must be symmetric when exchanging $t \leftrightarrow u$, where t and u are Mandelstam variables. Thus, we write the amplitude as $F(t) = f(t) + f(u)$ and thus an expression to fit the differential cross sections can be represented as:

$$d\sigma/dt = A^2 \ (e^{Bt/2} + e^{Bu/2})^2. \tag{4}$$

It is obvious that the parameterization can only be applied in a defined region of 4-momentum transfer, t. The region must not include a region where the Coulomb interaction dominates. Thus, we excluded experimental data with $|t| < 0.005$ (GeV/c)^2. The width of the region must be sufficiently large, because any data set could be fit with Eq. 4 for a narrow range of t. We choose a maximum value of $|t|$ equal to 0.125 (GeV/c)^2 as selected in reference [49].

Results[1)] of fits to the data (various symbols) within these t-ranges are presented in Fig. 1. The parameter A is observed to grow from $P_{lab} \simeq$ 1 GeV/c, reaches a maximum at $P_{lab} \simeq$ 1.7 GeV/c and then decreases at higher momentum (see Fig. 1a). Results for the COSY data are in a good agreement with the other data. A fit to only the EDDA data [48] gives acceptable results at $P_{lab} \leq$ 1.7 GeV/c. At higher P_{lab}, the parameter A for these data decreases, reflecting the fact that small angle data are absent in that measurement.

[1] $\chi^2/NDF = 938/642 \simeq 1.46$. Without fitting the EDDA data [48] and small angle data at P_{lab} = 9.43 and 18.9 GeV/c, $\chi^2/NDF = 533/579 \simeq 0.92$. NDF = Number of Degree of Freedom.

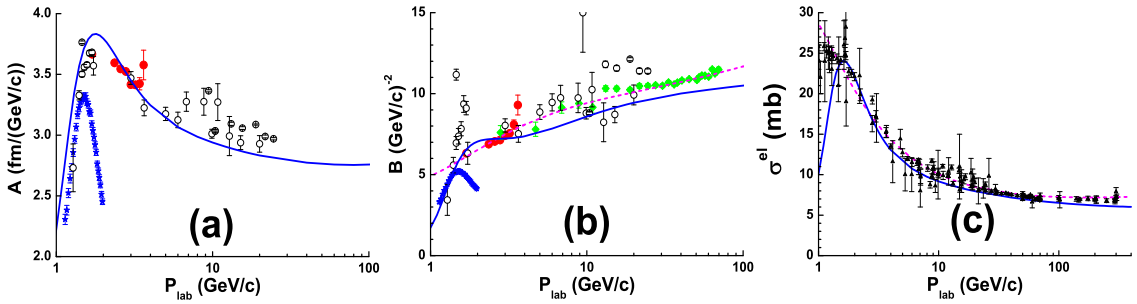

Figure 1: a, b) Fit parameters A and B as functions of the projectile momentum, P_{lab}. Open circles are results of the fit to the data [50] – [60]. Filled circles are the results for the latest COSY data [37]. Stars present results of the fit to the EDDA data [48]. Diamonds are data from reference [49] (see Fig. 1b). Dashed (magenta) curves are approximations of the dependencies. Descriptions of the solid curves are given in the text. c) Elastic cross section as a function of P_{lab}. The data points are from the PDG data-base [34].

The parameter B grows for $P_{lab} \geq 1$ GeV/c, and then sharply decreases above $P_{lab} \simeq 1.7$ GeV/c and continues with a smooth growth for higher momentum (see Fig. 1b). Our fit results are in agreement with previous ones [49] at $P_{lab} > 10$ GeV/c. The COSY data clarify the behaviour at $P_{lab} = 1.7 - 3.6$ GeV/c. The EDDA data cannot be used to determine these parameters for $P_{lab} > 1.7$ GeV/c, because they do not measure to sufficiently small momentum transfer.

If the fit and the data on σ_{pp}^{tot} and ρ_{pp} are self-consistent, then the parameter A must be connected with σ_{pp}^{tot} and ρ_{pp} according to Eq. 3. To check this we need parameterizations of σ_{pp}^{tot} and ρ_{pp}, because the momentum range of these data does not coincide with the range where σ_{pp}^{tot} and ρ_{pp} have been determined. Extending the PDG parameterizations [34], we approximate σ_{pp}^{tot} and ρ_{pp} by the following formulae:

$$\sigma_{pp}^{tot} = \sigma_{PDG}^{tot} + \frac{7200}{(s/s_0)^{3.5}} - \frac{32}{(s/s_0 - 4)^2 + 0.45} \quad \text{[mb]}, \tag{5}$$

$$\rho_{pp} = \rho_{PDG} + \frac{1.5}{(s/s_0)} - \frac{3}{(s/s_0)^2}, \quad s_0 = 1 \text{ GeV}^2, \tag{6}$$

where s is the center-of-mass energy squared ($s = 2m_N^2 + 2m_N(E + m_N)$) in GeV^2, m_N is the nucleon mass (0.938 GeV/c^2), and

$$\sigma_{PDG}^{tot} = H \ \ln^2(s/s_M) + P + R_1(s/s_M)^{-\eta_1} - R_2(s/s_M)^{-\eta_a 2}, \tag{7}$$

$$\rho_{PDG} = \frac{1}{\sigma_{PDG}^{tot}} \left[\pi H \ln(s/s_M) - R_1(s/s_M)^{-\eta_1} \tan\left(\frac{\eta_1 \pi}{2}\right) - R_2(s/s_M)^{-\eta_2} \cot\left(\frac{\eta_2 \pi}{2}\right) \right], \tag{8}$$

$$s_M = (2m_N + M)^2, \quad M = 2.076 \text{ [GeV]}, \quad H = 0.2838 \text{ [mb]}, \quad P = 33.73 \text{ [mb]},$$

$$R_1 = 13.67 \text{ [mb]}, \quad \eta_1 = 0.412, \quad R_2 = 7.77 \text{ [mb]}, \quad \eta_2 = 0.5626.$$

Experimental data on σ_{pp}^{tot} and ρ_{pp} from the PDG data-base are presented in Fig. 2 together with our parameterizations. The PDG parameters were determined at $\sqrt{s} \geq 7$ GeV. Direct extrapolations of the PDG parameterizations below 7 GeV are shown in Fig. 2 by dashed lines. It is obvious, that they do not describe the data in the low momentum domain. Thus, we include additional terms in our approximations.

The forms of the additional terms are mainly motivated by the reggeon phenomenology. According to the phenomenology, a yield of a non-vacuum reggeon exchange to the elastic scattering amplitude is proportional to $1/s^n$ at high momenta, where n can be ~ 0.5, 1, 1.5, 2 and so on for various reggeons. The PDG parameterization of the total cross sections include only two effective non-vacuum reggeon exchanges – terms $R_1(s/s_M)^{-\eta_1}$ and $R_2(s/s_M)^{-\eta_2}$.

We did not extend our parameterization for ρ_{pp} below 1 GeV/c, because the behavior of the ρ_{pp} data is unclear for these momenta.

The latest COSY data [37] helped to estimate ρ_{pp} in the momentum range 1.7 – 3.6 GeV/c. According to Eq. 3, $\rho_{pp} = -\sqrt{16\pi \ (A/\sigma_{pp}^{tot})^2 - 1}$. We calculated ρ_{pp} using the fit results for A and the approximation

for σ_{pp}^{tot} according to Eq. 5. The calculations are presented in Fig. 2 by stars. They clarify the behavior of ρ_{pp} at momenta below 3.8 GeV/c. After that, we determined parameters of the approximation in Eq. 6.

Having the approximations in Eqs. 5 and 6, we can now investigate Eq. 3 in the momentum range under study. The estimated values of A are presented by the solid line in Fig. 1a. As seen, the estimations are in reasonably good agreement with the fit results for $P_{lab} \leq 8$ GeV/c (i.e. the estimations do not deviate from experimental values by more than experimental error bars). The estimations are lower than the fit results by about 5 – 10 % for $P_{lab} = 8 - 25$ GeV/c. This can be connected with an overestimation of ρ_{pp} in the momentum region: $\rho_{pp} \simeq -0.35$ according to the Eq. 6. It is sufficient to reach an agreement between the estimations and the fit results for A to decrease ρ_{pp} down to -0.45 as it was for the COSY momenta. Thus, we believe that ρ_{pp} can have a non-trivial behavior in this momentum region. It could be a main reason why the high momentum approximation cannot be extended in the low momentum domain.

Of course, that disagreement could result from an over-simplified exponential expression. We evaluate this hypothesis in the next section.

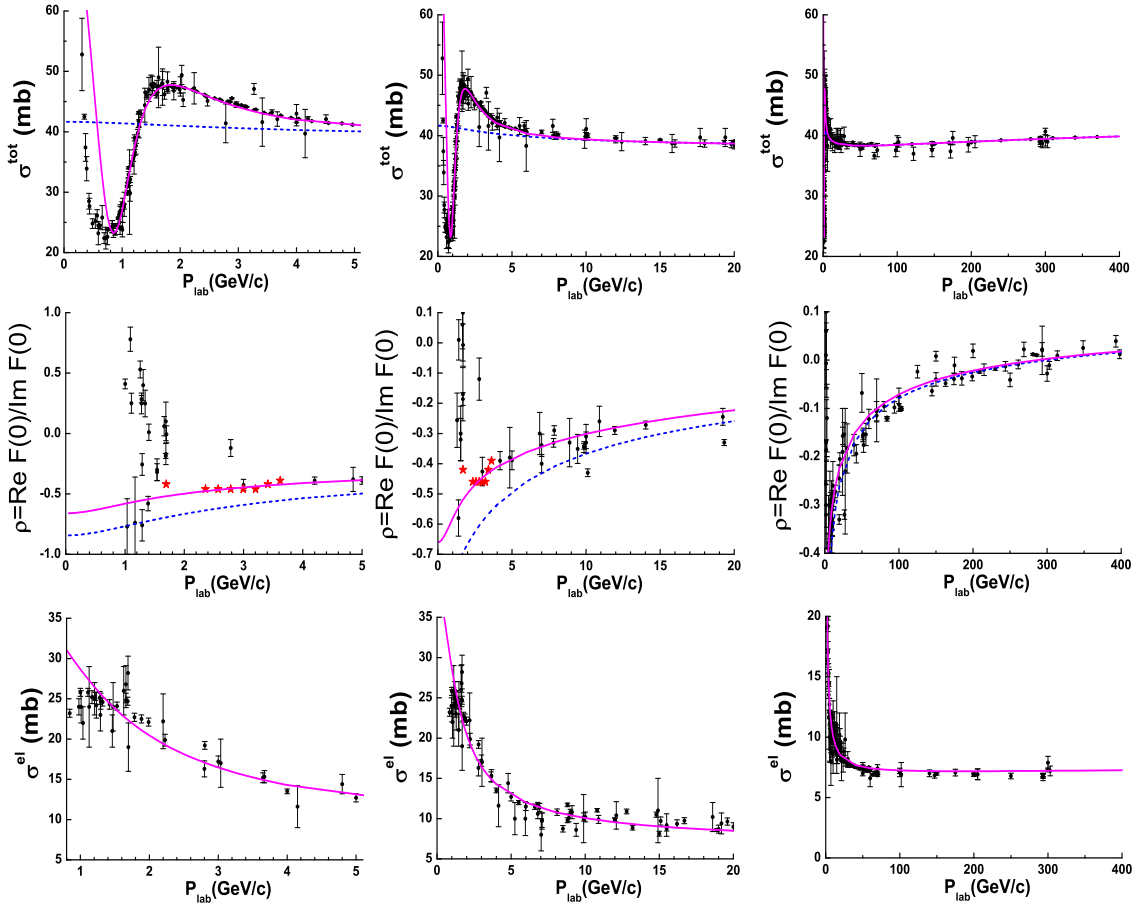

Figure 2: σ_{pp}^{tot}, σ_{pp}^{el} and ρ_{pp} as functions of P_{lab}. Points are data from PDG data-base [34]. Dashed lines are extrapolations of the PDG parameterizations. The solid lines are our approximations.

It is useful to have an approximation of the momentum dependence of the parameter B for the Glauber calculations of the differential cross sections. We parameterize the fit results for B by the following formula:

$$B = 1.9\ \ln(s/s_0) + \frac{27}{\sqrt{s/s_0}} - \frac{47}{(s/s_0)} \quad [(\mathrm{GeV/c})^{-2}]. \tag{9}$$

Calculations using this formula are shown as a dashed line in Fig. 1b.

Using the approximated values for A and B, we calculate the elastic cross sections ($\sigma_{pp}^{el} = |A|^2/B$) presented in Fig. 1c by a solid line. As expected, the calculations somewhat underestimate the cross

sections. To show this, we fit the elastic cross sections with the following expression:

$$\sigma_{pp}^{el} = 0.18\ \sigma_{PDG}^{tot} + \frac{60}{(s/s_0)} + \frac{600}{(s/s_0)^3} \quad \text{[mb]}, \tag{10}$$

and plot it in Fig. 1c as a dashed line. From the other hand, the approximations for σ_{pp}^{tot}, σ_{pp}^{el} and ρ_{pp} can be used to calculate B as

$$B = \frac{(\sigma_{pp}^{tot})^2(1+\rho_{pp}^2)}{16\ \pi\ \sigma_{pp}^{el}}\ 2.568 \quad [(\text{GeV/c})^{-2}], \tag{11}$$

if σ_{pp}^{tot} and σ_{pp}^{el} are given in millibarn. The calculated values of B are shown as a solid line in Fig. 1b. As seen, the calculations also underestimate the fit results. Note, that Eq. 11 allows one a correct reproduction of the inelastic cross sections.

2 Two exponential parameterization of pp data

The two exponential parameterization is considered in order to describe experimental data over a wide range of t.

$$\frac{d\sigma}{dt} = |A_1\ e^{B_1 t/2}\ +\ A_2 e^{i\phi}\ e^{B_2 t/2}|^2, \tag{12}$$

where A_1, B_1, A_2, B_2 and ϕ are real numbers. It was proposed in Ref. [38] for an analysis of anti-proton-proton elastic scattering data and was also applied to describe a wide set of $\bar{p}p$ data in the momentum range 1 – 15 GeV/c in [39, 40, 41].

This idea was independently proposed by R.J.N. Phillips and V.D. Barger [43] in 1973. They analyzed only pp experimental data at P_{lab} =12, 14.2, 19.2, 24, 29.7 GeV/c and at $\sqrt{s_{pp}} = 53$ GeV for the range $0.15 < |t| < 5$ (GeV/c)^2.

This paramterization has been used to fit the available experimental data within the range $0.005 < |t| < 5$ (GeV/c)^2. Results of the fit are presented in Tab. 1. The values of the parameters for the two restrictions on t ($0.15 < |t|$ [43] and $0.005 < |t|$ as before) differ by no more than 10 %. The typical difference is about 5 %. Our restriction allowed additional data sets to be included in the fitting procedure. The parameters have been constrained as in Ref. [41], because Eq. 12 contains 5 parameters

Table 1: Results of five-parameter fits with Eq. 12 for pp interactions.

P_{lab}	A_1	B_1	A_2	B_2	ϕ	χ^2/NDF
[GeV/c]	[fm/(GeV/c)]	[(GeV/c)$^{-2}$]	[fm/(GeV/c)]	[(GeV/c)$^{-2}$]	[rad]	
10.0	2.48 ± 0.08	7.85 ± 0.28	0.0790 ± 0.0190	1.20 ± 0.26	1.59 ± 0.24	0.93
12.0	2.76 ± 0.08	7.95 ± 0.20	0.0772 ± 0.0079	1.28 ± 0.09	1.73 ± 0.13	0.42
14.2	2.37 ± 0.11	7.77 ± 0.23	0.0948 ± 0.0066	1.67 ± 0.05	2.13 ± 0.08	0.23
19.2	2.67 ± 0.05	8.09 ± 0.09	0.7780 ± 0.0021	1.76 ± 0.02	2.11 ± 0.04	1.33
20.0	2.77 ± 0.02	8.51 ± 0.08	0.0682 ± 0.0064	1.72 ± 0.10	1.88 ± 0.07	1.56
21.12	2.52 ± 0.04	8.18 ± 0.11	0.0466 ± 0.0076	1.26 ± 0.18	1.93 ± 0.09	2.92
24.0	2.51 ± 0.05	7.98 ± 0.10	0.0707 ± 0.0030	1.84 ± 0.03	2.22 ± 0.05	0.62
29.7	2.56 ± 0.03	8.59 ± 0.13	0.0451 ± 0.0111	1.58 ± 0.26	2.09 ± 0.11	1.29
50	2.70 ± 0.01	9.60 ± 0.06	0.0189 ± 0.0023	1.60 ± 0.10	1.75 ± 0.10	2.59
200	2.48 ± 0.01	9.55 ± 0.03	0.0055 ± 0.0006	1.29 ± 0.07	2.33 ± 0.05	6.56
293	1.17 ± 0.08	7.67 ± 0.16	0.0207 ± 0.0024	2.04 ± 0.09	2.97 ± 0.02	0.90
501	2.42 ± 0.01	9.56 ± 0.19	0.0895 ± 0.0002	1.53 ± 0.02	2.95 ± 0.02	5.39

that are often strongly correlated. Due to the correlation the fit does not always converge. Thus, we have introduced a constraint to reduce the number of free parameters. Three of these constraints were considered in Ref. [41]: $B_1 = 10$ (GeV/c)$^{-2}$, $B_2 = B_1/3$ and $\phi = 2.793$. According to Tab. 1, B_1 varies by about ± 8 %, B_2/B_1 by about ± 42 %, and ϕ by about ± 16 %. Considering the fit results with the simple exponential expression (see Fig. 1b), it is difficult to assume that B_1 is a constant in the momentum range studied. B_2/B_1 also varies too strongly. Thus, we assume that ϕ is approximately

Table 2: Results of fits with Eq. 12 for pp interactions at ϕ =1.94 rad.

P_{lab}	A_1	B_1	A_2	B_2	χ^2/NDF
[GeV/c]	[fm/(GeV/c)]	[(GeV/c)$^{-2}$]	[fm/(GeV/c)]	[(GeV/c)$^{-2}$]	
5.5	13.15 ± 0.06	4.21 ± 0.12	0.208 ± 0.010	1.30 ± 0.04	2.13
10.0	24.12 ± 0.06	7.43 ± 0.10	0.117 ± 0.009	1.59 ± 0.10	1.01
12.0	26.91 ± 0.06	7.66 ± 0.09	0.090 ± 0.004	1.41 ± 0.05	0.53
14.2	25.34 ± 0.10	8.22 ± 0.14	0.084 ± 0.003	1.59 ± 0.03	0.46
18.4	26.76 ± 0.13	8.55 ± 0.23	0.239 ± 0.140	3.54 ± 0.96	0.87
19.2	27.60 ± 0.05	8.40 ± 0.06	0.071 ± 0.001	1.72 ± 0.01	1.90
20.0	27.61 ± 0.02	8.44 ± 0.03	0.072 ± 0.005	1.76 ± 0.09	1.53
21.12	25.12 ± 0.03	8.16 ± 0.05	0.048 ± 0.003	1.29 ± 0.07	2.70
24.0	25.99 ± 0.04	8.40 ± 0.07	0.060 ± 0.002	1.75 ± 0.02	1.53
29.7	25.76 ± 0.03	8.73 ± 0.05	0.035 ± 0.005	1.34 ± 0.17	1.30
50.0	26.86 ± 0.01	9.49 ± 0.03	0.022 ± 0.002	1.70 ± 0.08	2.64

constant and set it to an average value from Tab. 1, ϕ =1.94 rad, at $P_{lab} \leq 50$ GeV/c. We repeat the fit with a constant value of ϕ. Results of the fit are given in Tab. 2 and presented by solid points in Fig. 3.

As seen in Fig. 3, the results for the data at P_{lab} =5.5 GeV/c [53] and 10 GeV/c [58] are far off the other results. This is because the data at 5.5 GeV/c have no points for $|t| \leq 0.66$ (GeV/c)^2 (see Fig. 4a). Thus, the parameters A_1 and B_1 cannot be determined correctly. The experimental data at P_{lab} =5.5 GeV/c and data at P_{lab} =5.0 GeV/c [52] are plotted in Fig. 4a. The last data have points at small $|t|$ but do not have enough points at large $|t|$.

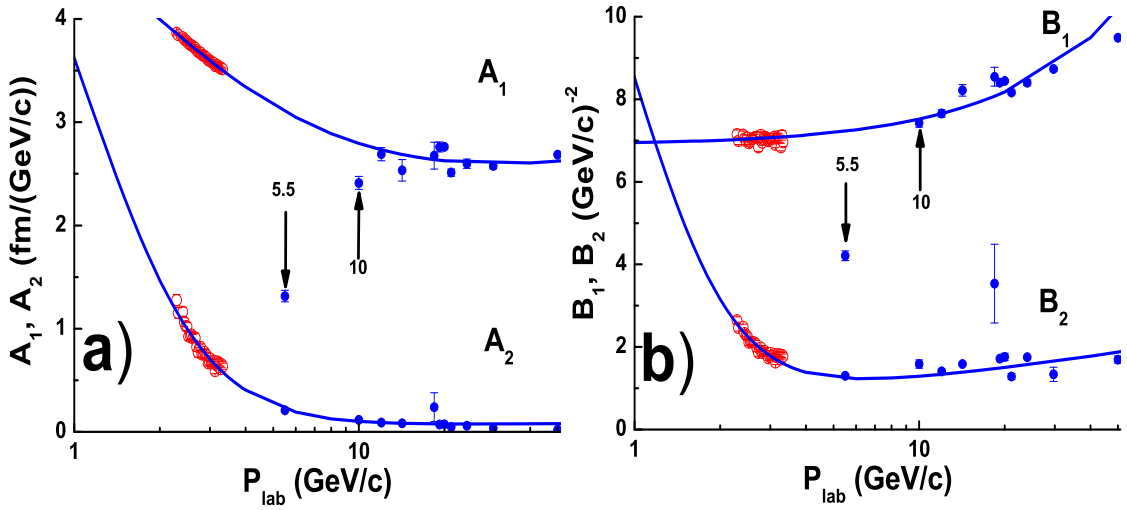

Figure 3: Fitted parameters A_1, A_2, B_1 and B_2 as functions of projectile momentum. Solid points (blue) are results of the fitting of the data [50] – [63] with constant ϕ. Open points (red) are results for the EDDA data [48]. Arrows mark the results for A_1 and B_1 at 5.5 and 10 GeV/c. Solid lines are approximations (see below).

A more complicated situation occurs at P_{lab} =10 GeV/c [58]. We compare those data with data at 9.9 GeV/c [56] in Fig. 4b. As seen, the data at 10 GeV/c do not have sufficient points at low $|t|$. In addition, the points at 10 GeV/c fluctuate more strongly than the data at 9.9 GeV/c. All of these reflect on the fit results.

To clarify the parameter's behaviour at P_{lab} <3 GeV/c, we have included the EDDA data into the fit. The fit does not converge because the data only contain differential cross section values at large scattering angles. To overcome the problem, we added values of $d\sigma/dt$ at $t = 0$ to the data. These values were calculated using σ_{pp}^{tot} and ρ_{pp} according to Eq. 5 and 6. Errors of the values were set 0.5 %. Results of the fit are presented by open points in Fig. 3.

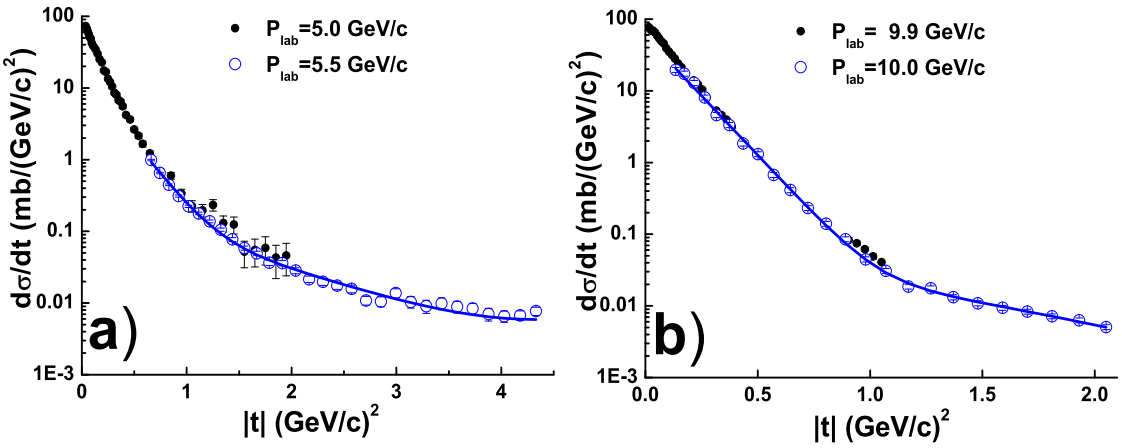

Figure 4: Differential cross sections at various momentum transfers. The solid points are reference data [52, 56], and the open points have been fit [52, 53, 58]. The blue solid lines are the results of the fit.

Future calculations require approximations of the momentum dependence of A_1, A_2, B_1 and B_2. A fit to the high momentum data ($\sqrt{s} > 23$ GeV) to Eq. 12 has been done in Refs. [45, 47], and they find that A_1 and B_1 smoothly grow in the range $23 < \sqrt{s} \leq 7000$ GeV. A_2 and B_2 have more complicated behaviour, however the following simple behaviours were proposed in Ref.[47]:

$$A_1 = a\ (s/s_0)^{-\epsilon_1} + b\ (s/s_0)^{\epsilon_2}, \quad A_2 = c\ (s/s_0)^{-\epsilon_3} + d\ (s/s_0)^{\epsilon_4}, \tag{13}$$

$$B_1 = b_0 + b_1 \ln(s/s_0), \quad B_2 = b_2 + b_3 \ln(s/s_0). \tag{14}$$

We were not able to select the parameters of Eq. 14 in the momentum range studied. Thus, we changed the expressions for B_1 and B_2 to:

$$B_1 = b_0\ (s/s_0)^{-\epsilon_5} + b_1\ (s/s_0)^{\epsilon_6}, \quad B_2 = b_2\ (s/s_0)^{-\epsilon_7} + b_3\ (s/s_0)^{\epsilon_8}. \tag{15}$$

A careful selection of the parameters of the expressions resulted in:

$$a = 10.6\ [\mathrm{fm/(GeV/c)}], \quad \epsilon_1 = 0.9, \quad b = 1.55\ [\mathrm{fm/(GeV/c)}], \quad \epsilon_2 = 0.1 \tag{16}$$

$$c = 290\ [\mathrm{fm/(GeV/c)}], \quad \epsilon_3 = 3, \quad d = 0.05\ [\mathrm{fm/(GeV/c)}], \quad \epsilon_4 = 0.1 \tag{17}$$

$$b_0 = 6.8\ [(\mathrm{GeV/c})^{-2}], \quad \epsilon_5 = 0., \quad b_1 = 0.035\ [(\mathrm{GeV/c})^{-2}], \quad \epsilon_6 = 1.0 \tag{18}$$

$$b_2 = 2700\ [(\mathrm{GeV/c})^{-2}], \quad \epsilon_7 = 4, \quad b_3 = 0.6\ [(\mathrm{GeV/c})^{-2}], \quad \epsilon_8 = 0.25 \tag{19}$$

Having the approximations, we can corroborate the self-consistency of the fit. Neglecting the $t \leftrightarrow u$ symmetry at sufficiently high momenta, a general form of the two exponential parameterization can be represented as

$$F(t) = e^{i\phi_0}\ [A_1\ e^{B_1 t/2}\ +\ A_2 e^{i\phi}\ e^{B_2 t/2}]. \tag{20}$$

Thus,

$$\sigma^{tot} = 4\pi\ Im(F(0)) = 4\pi\ \{\sin(\phi_0)\ [A_1 + A_2\cos(\phi)] + A_2\cos(\phi_0)\sin(\phi)\}\ \frac{1.974}{\sqrt{\pi}} \quad [\mathrm{mb}], \tag{21}$$

$$\phi_0 = \pi\ + \arctan\left\{\frac{[A_1 + A_2\cos(\phi)] - \rho A_2 \sin(\phi)}{\rho[A_1 + A_2\cos(\phi)] + A_2\sin(\phi)}\right\}. \tag{22}$$

Using ρ_{pp} given by Eq. 6 and approximations of the parameters, we have calculated σ^{tot}_{pp} and confirmed that the obtained values coincide with ones predicted by Eq. 5 to the level of $\pm$ 5 %. It is a typical precision of our estimations. New, more accurate experimental data on pp elastic scattering are needed in order to increase the precision.

3 Parameterization of the np elastic scattering amplitude

General properties of the np interaction – σ_{np}^{tot}, σ_{np}^{el} and ρ_{np} are presented in Fig. 5 together with our approximations for pp collisions. The total np cross section is lower than the pp cross section for $P_{lab} = 1.2 - 3.4$ GeV/c. They aproach each other at higher momenta. The data on total cross sections of pn and np interactions are different in the region $P_{lab} = 1.2 - 2.2$ GeV/c. It is a consequence of the different methods applied for the measurements and the complicated structure of the differential cross section. We will not consider the difference in detail, but we will assume that the pn data are more precise than np ones.

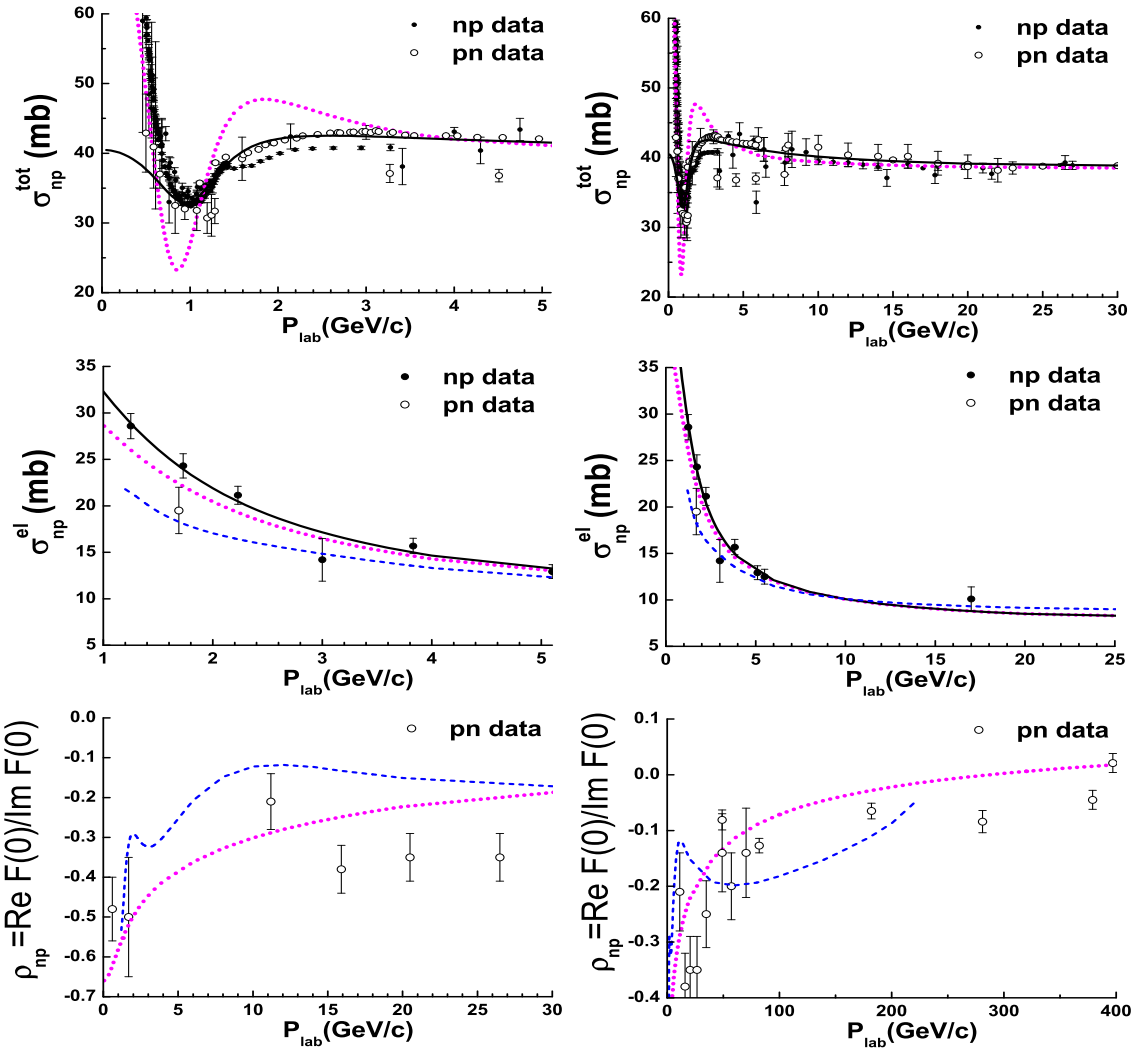

Figure 5: σ^{tot}, σ^{el} and ρ of pn and np interactions as functions of P_{lab}. The data points are from [34]. Solid (black) lines are approximations for pn and np interactions. Dotted (magenta) lines are our approximations for pp interactions. Dashed (blue) lines are calculations (see the text).

As also seen in the figure, the total elastic scattering cross section for np interactions is larger than the analogous data for pp collisions at $P_{lab} \leq 3.3$ GeV/c. There is not sufficient data on $\rho = Re(F(0))/Im(F(0))$ for np interactions to draw a solid conclusion. Nevertheless, since they generally agree with pp data, we have assumed that $\rho_{np} = \rho_{pp}$.

Because the properties of np interactions are similar to those of pp interactions, we approximate the momentum dependence of both σ_{np}^{tot} and σ_{np}^{el} by expressions analogous to Eqs. 5 and 10 with an additional terms.

$$\sigma_{np}^{tot} = \sigma_{PDG}^{tot} + \frac{18}{(s/s_0)} - \frac{6.4}{(s/s_0 - 4.25)^2 + 0.5} \quad \text{[mb]}, \tag{23}$$

$$\sigma_{np}^{el} = 0.18\ \sigma_{PDG}^{tot} + \frac{60}{(s/s_0)} + \frac{900}{(s/s_0)^3} \quad \text{[mb]}, \tag{24}$$

where σ_{PDG}^{tot} is given by Eq. 7.

We start out by describing the np differential cross sections with the standard one exponential parameterization. Using a restriction on $|t|$ as in the case of pp scattering ($|t| < 0.125$ (GeV/c)^2) we found only one data set [64] at $P_{lab} = 0.924 - 1.793$ GeV/c containing the necessary points. Since that data set was not sufficient for the fit, we increased the upper limit of $|t|$ to 0.25 (GeV/c)^2 using the data [64] – [71] but were not satisfied by the fit results because they could not allow to determine the momentum dependence of the parameters. Various restrictions on the fit range of t were used in the literature [65, 68, 66, 72, 73]. Very often a value for the maximum $|t|$ of 0.5 (GeV/c)^2 was considered. Fit results of Eq. 1 to the experimental data with this upper limit are shown in Fig. 6.

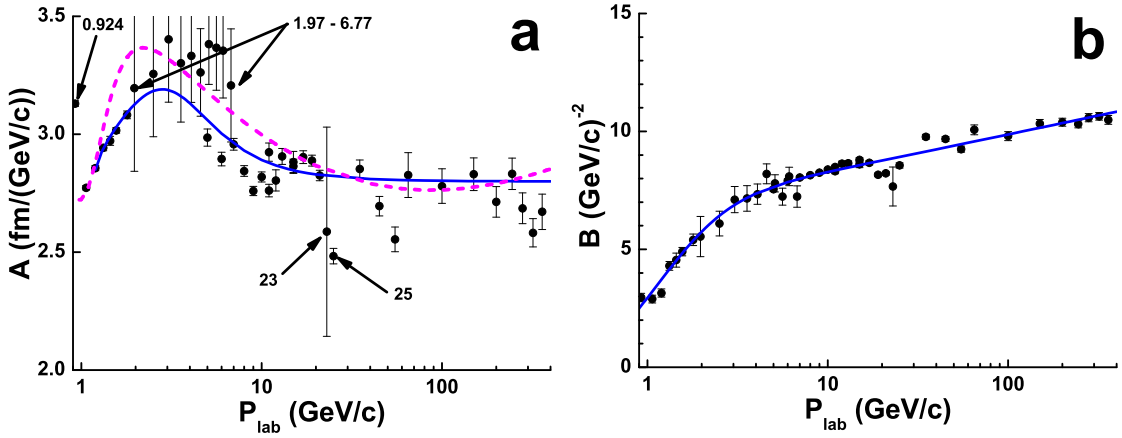

Figure 6: Fit results of Eq. 1 to np differential elastic scattering cross sections [64] – [71] at $|t| <$ 0.5 (GeV/c)^2. Points are the fit results. Solid lines are approximations (Eqs. 25 and 26). For a description of the dashed line see the text.

Three problems arise: 1 – the parameter A at P_{lab} =0.924 GeV/c is much larger than the parameters at similar momenta; 2 – points at P_{lab} =1.97 – 6.77 GeV/c have large error bars; 3 – values of A at P_{lab} =23 and 25 GeV/c are lower than the other values. In addition, the point at P_{lab} =23 GeV/c has large error bars, and there is a large $\chi^2/NDF = 7.82$ at P_{lab} =9 GeV/c. The problematic points are marked by arrows in Fig. 6.

The large error bars at P_{lab} =1.97 – 6.77 GeV/c are connected with the small number of experimental points included in the fit, only 4 points for each data set. The same is true at P_{lab} =23 GeV/c. Only 5 data points were considered for that fit. Of course, the number of included data points can be increased by increasing the maximum value of the allowed $|t|$ range, but this systematically effects the values of B.

A more complicated situation takes place with other problems (see Fig. 7). Fluctuation of experimental data points [64] at P_{lab} =0.924 and 1.065 GeV/c presented in Fig. 7a are comparable to each other. Relative error bars of the data are also comparable. The only essential difference is the magnitudes. The difference was noted in Ref. [64], but no explanation was given. The data at P_{lab} =0.924 GeV/c also are above the phase-shift analysis results as shown in Ref. [64]. Thus, we decided to exclude the fit results at P_{lab} =0.924 GeV/c from our consideration.

We show experimental data [69] at P_{lab} =15, 25 and 35 GeV/c together with fit results in Fig. 7b. As seen, the slope parameter increases going from 15 to 35 GeV/c. The B values at 15 and 25 GeV/c are comparable. At the same time the maximum value of $d\sigma/dt$ (at $|t| < 0.23$ (GeV/c)^2) decreases going from 15 to 25 GeV/c, and suddenly increases going to 35 GeV/c. This behavior was not noted in Ref. [69]. Maybe it was not essential because the absolute normalization error was estimated to be $\sim 35\%$ [69]. We did not consider systematic errors in our fit. Because the fit results at P_{lab} =25 GeV/c fall outside of the common trend, we do not take them into account.

We show in Fig. 7c experimental data [67] at two similar momenta, 9 and 10 GeV/c together with our fit results. The data are similar, except data points at $|t|$ =0.13 and 0.145 (GeV/c)^2 at P_{lab} =9 GeV/c (marked by arrows). They give the largest contribution to χ^2. The other similar data point is also marked in the figure. Because the general properties of the distributions are similar, we consider the

large χ^2/NDF at $P_{lab} = 9$ GeV/c to be a consequence of the data quality and omission of the systematic errors.

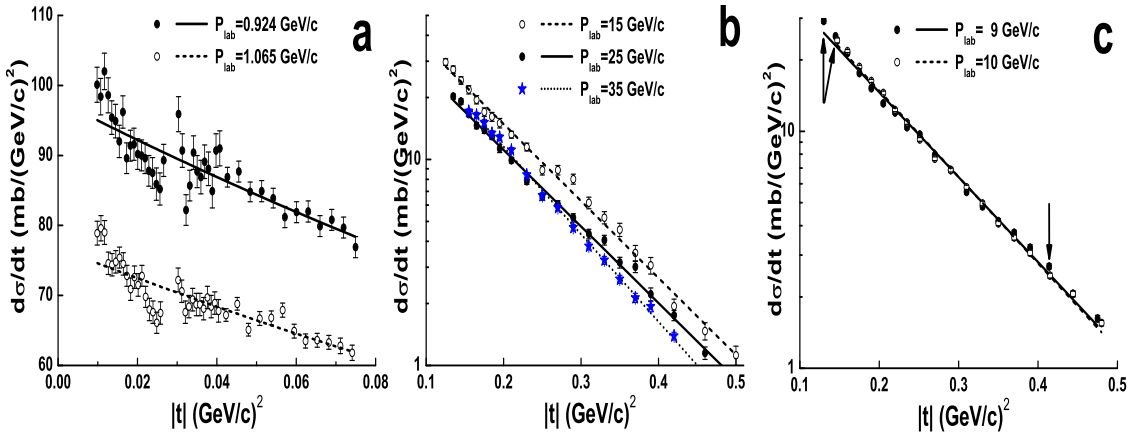

Figure 7: Data points are from Refs. [64], [69], [67] for Figs. a, b and c, respectively. Lines are fit results described in the text.

The fit results are connected with the fundamental properties of np interactions – σ_{np}^{tot}, σ_{np}^{el} and ρ_{np}. According to Eq. 3, A can be calculated as $A = \sigma_{np}^{tot}\sqrt{1+\rho_{np}^2}/(4\sqrt{\pi})$. The calculations with the assumption $\rho_{np} = \rho_{pp}$ are shown in Fig. 6a by the dashed line. As seen, the calculations deviate from the fit results, especially for $P_{lab} \leq 10$ GeV/c. We used Eq. 23 as an approximation for σ_{np}^{tot}, and Eq. 6 for ρ_{np}. At the same time, having σ_{np}^{tot} we can calculate ρ_{np} using Eq. 3 and the following approximation for A:

$$A = 2.8 + 6\,\frac{\sqrt{s/s_0 - 4\cdot 1.072}}{(s/s_0-5)^2+20} \quad [\mathrm{fm}/(\mathrm{GeV/c})]. \tag{25}$$

The calculations of ρ_{np} are shown by dashed lines in Fig. 5, and is seen to differs from ρ_{pp}. Consequently, our results show that a standard assumption, $\rho_{np} = \rho_{pp}$, is not correct.

Having A and B given by Eqs. 25 and 26, we can estimate σ_{np}^{el} as A^2/B. In doing this B is approximated by:

$$B = 6.2 + 0.7\ln(s/s_0) - \frac{350}{(s/s_0)^3} \quad [(\mathrm{GeV/c})^{-2}]. \tag{26}$$

The estimations of σ_{np}^{el} are shown by the dashed line in Fig. 5. As seen, they underestimate the cross section at $P_{lab} \leq 5$ GeV/c. This was expected because the standard parameterization cannot describe the cross sections at large momentum transfer. Thus, we consider the two exponential parameterization.

Typical differential cross section distributions of np elastic scattering are shown in Fig. 8a and have two maxima at forward and backward directions in the center-of-mass reference frame, at $t \sim 0$ and $t \sim t_{max}$. The backward peak appears due to the charge exchange reaction, $n+p \to p+n$. It is assumed that the backward peak is connected with π-meson exchange in the t channel (see references in [74]). The backward peak is located at $|u| < 0.025$ (GeV/c)^2 ($u = t_{max} - t$), and it is much smaller than the forward peak. Thus, we will not consider it in the following.

The forward peak is located at $|t| \leq 0.5$ (GeV/c)^2 [67]. There is a change of slope at $|t| \sim 1.5$ (GeV/c)^2, and a plateau at $0.3\cdot|t_{max}| \leq |t| \leq 0.7\cdot|t_{max}|$. It is obvious that the two exponential parameterization cannot describe the plateau. Thus, we modify the parameterization to be:

$$\frac{d\sigma}{dt} = |A_1\ e^{B_1 t/2}\ + e^{i\phi}(A_2\ e^{B_2 t/2} + A_3)|^2. \tag{27}$$

A fit of Eq. 27 to the experimental data of Refs. [66, 67] at $0.3\cdot|t_{max}| \leq |t| \leq 0.7\cdot|t_{max}|$ and $A_1 = A_2 = 0$ shows that the height of the plateau decreases as the momentum increases, and can be described by:

$$A_3 = 2000/(s/s_0)^{4.75} \quad [\mathrm{fm}/(\mathrm{GeV/c})]. \tag{28}$$

The plateau corresponds to isotropic scattering in the center-of-mass reference frame. Its yield in the differential cross section distributions are shown in Fig. 8a by solid and dashed lines.

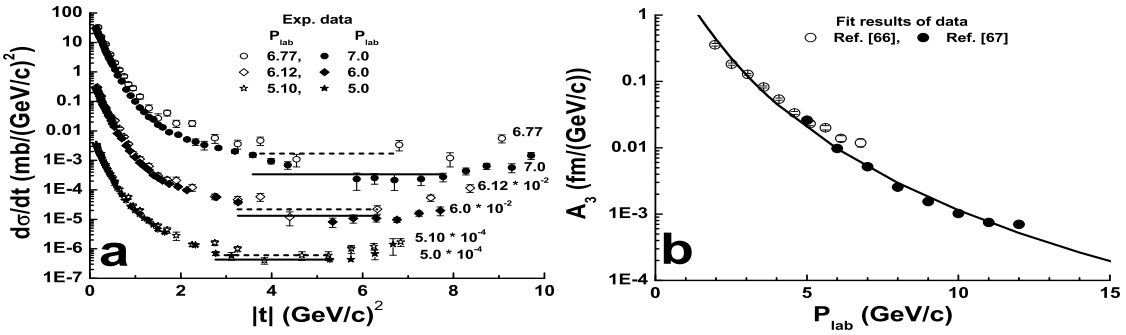

Figure 8: a) Differential cross section distributions of np elastic scattering at P_{lab} = 5.1, 6.12 and 6.77 GeV/c [66] (open points) and at P_{lab} = 5, 6 and 7 GeV/c [67] (closed points). Dashed and solid lines are fit results by Eq. 27 with $A_1 = A_2 = 0$ to the data [66] and [67], correspondingly. b) A_3 values from the fits to the data. The solid line is Eq. 28.

As seen in Fig. 8b, the fit results to the data [66, 67] differ. To understand the source of the difference we plotted the differential cross sections of Refs. [66, 67] at similar projectile momenta in Fig. 8a. As seen, the data of Ref. [66] are less precise than the data of Ref. [67] in the region of the plateau. The data in [66] vary more stronger than the data in [67]. The data are quite close to each other only at $P_{lab} \sim$ 5 GeV/c. Thus, we mainly followed the data of Ref. [67] to fulfill Eq. 28, shown in Fig. 8b by a solid line.

A two exponential fit of Eq. 27 to the data [64, 66, 67, 69, 70] using Eq. 28 gives meaningful results only for 22 of 45 sets of data. This is a consequence of the strong correlation of the parameters. According to the fit, an average value of ϕ is equal to 1.6. In order to reduce the correlations, we fixed ϕ to that value. With that constraint 39 data sets could be included. The fit results are shown in Fig. 9.

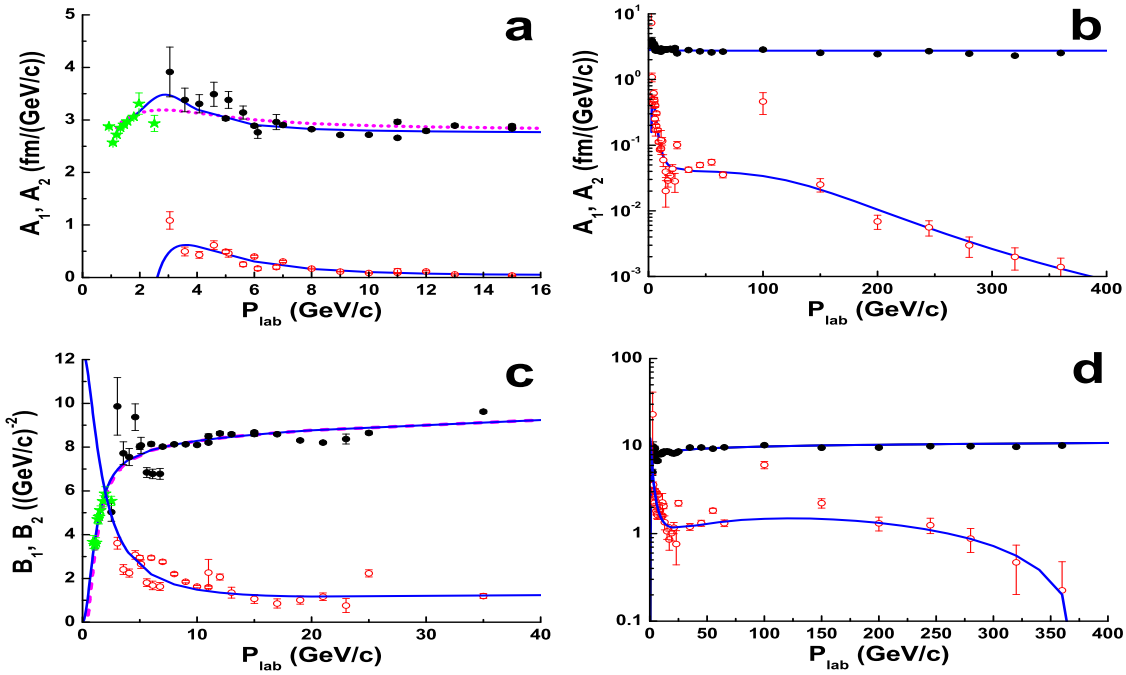

Figure 9: Fit results of Eq. 27 to the data [66]–[70]. Points are the fit results. Stars (green) are the results of fitting of Eq. 27 with $A_2 = 0$ to the data [64]. Solid lines are approximations (see below). Dashed lines are approximations of the A and B parameters of the one exponential expression.

The fit to the data of Ref. [64] at P_{lab} = 0.924 – 1.793 GeV/c gives too large values of A_1 and B_1, which are needed to reproduce the data at $|t| < 0.027$ (GeV/c)^2 (see Fig. 7a). The large values of A_2 and B_2 of the fit allow the data at $|t| > 0.03$ (GeV/c)^2 to be described. The errors of the parameters are also large. As seen in Fig. 7a, there is an empty region at $0.027 < |t| < 0.03$ (GeV/c)^2. We believe that

the region is a reflection of special features of the experiment, which also leads to a difference between the cross sections before and after the region. Taking all of these points into account, we conclude that the fit results are not realistic and thus we do not show them in Fig. 9.

At the same time, the data [64] are fit quite well by Eq. 27 with $A_2 = 0$ and A_3 given by Eq. 28. Those results are indicated by stars in Fig. 9. The parameters A_1 and B_1 in this case are rather close to the results of the one exponential parameterization fit.

The data of Ref. [66] at $P_{lab} = 1.97$ and 2.51 GeV/c do not have sufficient points at large $|t|$ (see Fig. 10a) for a good determination of the parameters. Thus, we fit Eq. 27 with $A_2 = 0$ to them as before. The fit results are also shown in Fig. 9 by stars.

The fit results of the data [66] at P_{lab} =3.05, 3.57, 4.08, 4.59, 5.10, 6.12 and 6.77 GeV/c have large error bars. The results are much better for the data [67] at P_{lab} =5, 6, 7, 8, 9, 10, 11 and 12 GeV/c.

The data of Ref. [69] at $P_{lab} = 15$ GeV/c could not be fit at all due to the restricted range of t (see Fig. 10e). The peculiarity of the data [69] at $P_{lab} = 25$ GeV/c was considered before. They lead to A_2 and B_2 values that are not consistent with other data sets.

The restricted range of t reflected on the fit results of data [70] at $P_{lab} = 100$ GeV/c (see Fig. 10f). At higher momenta all parameters regularly decrease with encreasing momentum, up to $P_{lab} = 360$ GeV/c.

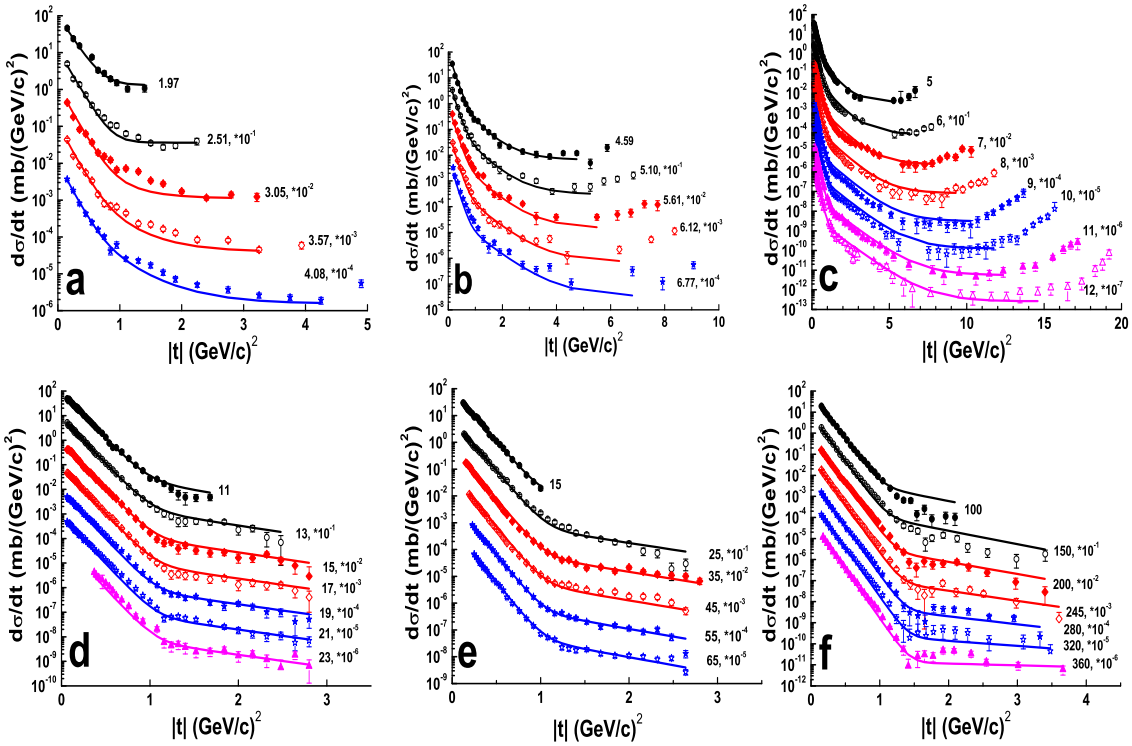

Figure 10: Description of np elastic differential cross sections by Eq. 27 with approximations 29 – 32. Points are experimental data [66, 67, 69, 70]. The experimental errors displayed are statistical only. Lines are calculation results.

Taking into account everything above, we propose the following approximation for the momentum dependence of the parameters at $P_{lab} \geq 2.5$ GeV/c:

$$A_1 = 2.75 + 2.25\ \frac{\sqrt{s/s_0 - 4.3}}{(s/s_0 - 7)^2 + 5} - 1.4\ 10^7/(s/s_0)^{12} \quad [\mathrm{fm}/(\mathrm{GeV/c})], \tag{29}$$

$$A_2 = 1.7\ 10^4\ (s/s_0 - 7)/(s/s_0)^5 + 0.04/[1.4\ 10^{-10}(s/s_0)^4 + 1] \quad [\mathrm{fm}/(\mathrm{GeV/c})], \tag{30}$$

$$B_1 = \ 6.2 + 0.7\ \ln(s/s_0) - 310/(s/s_0)^3 \quad [(GeV/c)^{-2}], \tag{31}$$

$$B_2 = 2\ 10^{-4}\sqrt{s/s_0}\ (715 - s/s_0) + 80/(s/s_0)^{1.5} \quad [(GeV/c)^{-2}]. \tag{32}$$

These parameters allow general features of the differential cross sections of np elastic scattering starting from 400 MeV up to 360 GeV to be described. The description is shown in Fig. 10. The total χ^2/NDF

for all data sets is equal 14740/1290∼11 without considering the systematic uncertainties since these are either not consistently provided, or in some cases not at all. For example, 4–7 % uncertainty in absolute normalization is given in Ref. [64], 10–20 % – in Ref. [66], +5 – -15 % – in Ref. [70]. We have used average values in these cases. Taking into account such uncertainties we have obtained $\chi^2/NDF = 4938/979 \sim 5$, which is vastly improved.[2]

The worst χ^2/NDF is observed for the data [70] at $P_{lab} \geq 100$ GeV/c. A separate fit of the data gives an acceptable χ^2/NDF, A_1 and B_1 which deviate from the corresponding approximations in the range by ± 5 %. Fitted values of A_2 and B_2 vary in a larger interval. The uncertainty of the A_2 values is ∼ 25 %, and errors of B_2 are on the level ∼ 50 – 70 %. This is understandable because the data do not include points with large momentum transfer. Thus, A_2 and B_2 cannot be determined as well in that momentum range. At the same time, our approximations allow the forward peak to be described sufficiently well.

Conclusions

- A general description of *pp* and *np* elastic scattering in the beam momentum range 2 – 50 GeV/c has been reached.
- 133 and 45 sets of experimental data on *pp* and *np* elastic scattering, respectively, were analyzed and fit.
- Two popular parameterizations of differential cross sections – a standard one exponential parameterization and the two coherent exponential parameterization, were used to fit the experimental data.
- Analytical expressions to approximate the momentum dependence of the fit parameters were proposed.
- Approximations of σ^{tot}, σ^{el} and ρ have also been proposed.

All of these give a solid base for effective Glauber calculations and Monte Carlo simulations of properties of nucleon-nucleon, nucleon-nucleus and nucleus-nucleus interactions at high momenta especially for FAIR and NICA, and for the RHIC Beam Energy Scan program.

The authors are thankful to D. Mchedlishvili for providing us with COSY data in a tabulated form, and O.V. Selyugin and N.I. Kochelev for useful discussions of the subject of the paper.

References

[1] G.D. Alkhazov, S.L. Belostotsky, and A.A. Vorobyov, Phys. Rep. **C42**, 89 (1978).

[2] J.S. Al-Khalili, J.A. Tostevin, and I.J. Thompson, Phys. Rev. **C54**, 1843 (1996).

[3] B. Abu-Ibrahim, K. Fujimura, and Y. Suzuki, Nucl. Phys. **A657**, 391 (1999).

[4] B. Abu-Ibrahim and Y. Suzuki, Phys. Rev. **C61**, 051601 (2000); **C62**, 034608 (2000).

[5] G.D. Alkhazov *et al.*, Nucl. Phys. **A712**, 269 (2002).

[6] P. Egelhof *et al.*, Eur. Phys. J. **A15**, 27 (2002).

[7] W. Horiuchi, Y. Suzuki, B. Abu-Ibrahim, and A. Kohama, Phys. Rev. **C 5**, 044607 (2007).

[8] B. Abu-Ibrahim, W. Horiuchi, A. Kohama, and Y. Suzuki, Phys. Rev. **C77**, 034607 (2008).

[9] C. Merino, I.S. Novikov, and Yu.M. Shabelski, Phys. Rev. **C80**, 064616 (2009).

[10] J. Zenihiro al., Phys. Rev. **C82**, 044611 (2010).

[11] A. Kohama, B. Abu-Ibrahim, W. Horiuchi, S. Iwasaki, and Y. Suzuki, Mod. Phys. Lett. **A25**, 1963 (2010).

[2] We did not include in the fit the data of Ref. [68] because the systematic uncertainty was not presented in the paper.

[12] G.D. Alkhazov, Yu. Shabelski, and I.S. Novikov, Int. J. Mod. Phys. **E20**, 583 (2011).

[13] W. Horiuchi, T. Inakura, T. Nakatsukasa, and Y. Suzuki, Phys. Rev. **C86**, 024614 (2012).

[14] W. Horiuchi, Y. Suzuki, and T. Inakura, Phys. Rev. **C89**, 011601 (2014).

[15] D. Chauhan, Z.A. Khan, and A.A. Usmani, Phys. Rev. **C90**, 024603 (2014).

[16] L.X. Chung, O.A. Kiselev, D.T. Khoa, and P. Egelhof, Phys. Rev. **C92**, 034608 (2015).

[17] G.D. Alkhazov, A.A. Vorobyov, A.V. Dobrovolsky, A.G. Inglessi, G.A. Korolev, and A.V. Khanzadeev, Phys. Atom. Nucl. **78**, 381 (2015), Yad. Fiz. **78**, 411 (2015).

[18] R.M. De Vries and J.-C. Peng, Phys. Rev. **C22**, 1055 (1980).

[19] D. Chauhan and Z.A. Khan, Phys. Rev. **C75**, 054614 (2007).

[20] B. Alver, M. Baker, C. Loizides and P. Steinberg, arXiv:0805.4411 [nucl-exp] (2005).

[21] M.L. Miller, K. Reygers, S.J. Sanders, and P. Steinberg, Annu. Rev. Nucl. Part. Sci. **57**, 205 (2007).

[22] L. Ray, Phys. Rev. **C20**, 1857 (1979).

[23] M.A. Zhusupov and E.T. Ibraeva, Phys. Part. Nucl. **31**, 723 (2000), Fiz. Elem. Chast. Atom. Yadra **31**, 1427 (2000).

[24] R.A. Arndt, L.D. Roper, R.A. Bryan, R.B. Clark, B.J. VerWest, and P. Signell, Phys. Rev. **D28**, 97 (1983).

[25] R.A. Arndt, I.I. Strakovsky, R.L. Workman, Phys. Rev. **C50**, 2731 (1994).

[26] R.A. Arndt, C.H. Oh, I.I. Strakovsky, R.L. Workman, F. Dohrmann, Phys. Rev. **C56**, 3005 (1997).

[27] J. Bystricky, C. Lechanoine-LeLuc, and F. Lehar, Eur. Phys. J. **C4**, 607 (1998).

[28] R.A. Arndt, I.I. Strakovsky, R.L. Workman, Phys. Rev. **C62**, 034005 (2000).

[29] R.A. Arndt, W.J. Briscoe, I.I. Strakovsky, and R.L. Workman, Phys. Rev. **C76**, 025209 (2007).

[30] R.A. Arndt, W.J. Briscoe, A.B. Laptev, I.I. Strakovsky, and R.L. Workman, Nucl. Sci. Eng. **162**, 312 (2009).

[31] http://gwdac.phys.gwu.edu/

[32] I. Frohlich *et al.*. PoS ACAT2007 076 (2007), Conference: C07-04-23.1 Proceedings; e-Print: arXiv:0708.2382 [nucl-ex].
M.A. Kagarlis, GSI Report 3, July 2000.

[33] S. Agostinelli *et al.* (Geant4 Collaboration), Nucl. Instrum. Methods **A506**, 250 (2003);
J. Allison *et al.* (Geant4 Collaboration), IEEE Trans. Nucl. Sci. **53**, 270 (2006).

[34] K.A. Olive *et al.* (Particle Data Group), Chin. Phys. **C38**, 090001 (2014); http://pdg.lbl.gov/

[35] V.A. Okorokov, Adv. High Energy Phys. **2015**, 914170 (2015).

[36] A. Sibirtsev, J. Haidenbauer, H.-W. Hammer, S. Krewald, and U.-G. Meisner, Eur. Phys. J. **A45**, 357 (2010).

[37] D. Mchedlishvili *et al.*, Phys. Lett. **B755**, 92 (2016).

[38] G.R. Kalbfleisch, R.C. Strand, and V. Vanderburg, Nucl. Phys. **B30**, 466 (1971).

[39] H.B. Crawley, E.S. Hafen and W.J. Kerman, Phys. Rev. **D8**, 2012 (1973).

[40] H.B. Crawley, W.J. Kerman and F. Ogino, Phys. Rev. **D8**, 2781 (1973).

[41] H.B. Crawley, N.W. Dean, E.S. Hafen, W.J. Kerman, and F. Ogino, Phys. Rev. **D9**, 189 (1974).

[42] A. Galoyan, J. Ritman, A. Sokolov, and V. Uzhinsky, arXiv:0809.3804 [hep-ex].

[43] R.J.N. Phillips and V.D. Barger, Phys. Lett. **B46**, 412 (1973).

[44] A. Grau, S. Pacetti, G. Pancheri, and Y. N. Srivastava, Phys. Lett. **B714**, 70 (2012).

[45] D. A. Fagundes *et al.*, Phys. Rev. **D88**, 094019 (2013).
D. A. Fagundes *et al.*, Proc. Sci, DIS (2013) 306.

[46] G. Pancheri *et al.*, Nuov. Cim. Soc. Ital. Fis. **037**, 179 (2014).

[47] A. Ster, L. Jenkovszky, and T. Csorgo, Phys. Rev. **D91**, 074018 (2015).

[48] D. Albers *et al.* (EDDA Collaboration), Eur. Phys. J. **A22**, 125 (2004);
http://www.iskp.uni-bonn.de/gruppen/edda

[49] G.G. Beznogikh *et al.*, Phys. Lett. **B30**, 274 (1969).

[50] A.V. Dobrovolsky *et al.*, Nucl. Phys. **B214**, 1 (1983).

[51] F. Irom *et al.*, Phys. Rev. **C25**, 373 (1982).

[52] I. Ambats *et al.*, Phys. Rev. **D9**, 1179 (1974).

[53] R.C. Kammerud *et al.*, Phys. Rev. **D**4, 1309 (1971).

[54] K.J. Foley *et al.*,Phys. Rev. Lett. **11**, 425 (1963).

[55] G.G. Beznogikh *et al.*, Nucl. Phys. **B54**, 78 (1973).

[56] R.M. Edelstein *et al.*, Phys. Rev. **D5**, 1073 (1972).

[57] G.W. Brandenburg *et al.*, Phys. Lett. **B58**, 367 (1975).

[58] J.V. Allaby *et al.*, Nucl. Phys. **B52**, 316 (1973).

[59] D. Harting *et al.*, Nuovo Cim. **38**, 60 (1965).

[60] J.V. Allaby *et al.*, Phys. Lett. **B28**, 67 (1968).

[61] Z. Asad *et al.*, Nucl. Phys. **B255**, 273 (1985).

[62] C.W Akerlof *et al.*, Phys. Rev. **D14**, 2864 (1976).

[63] U. Amaldi and K.R. Schibert, Nucl. Phys. **B166**, 301 (1980).

[64] Y. Terrien *et al.*, Phys. Rev. Lett. **59**, 1534 (1987).

[65] M.N. Kreisler *et al.*, Phys. Rev. Lett. **16**,1217 (1966).

[66] M.L. Perl, J. Cox, M.J. Longo, and M. Kreisler, Phys. Rev. **D1**, 1857 (1970).

[67] J.L. Stone *et al.*, Phys. Rev. Lett. **38**, 1315 (1977).

[68] J. Engler *et al.*, Nucl. Phys. **B62**, 160 (1973).

[69] V. Bohmer *et al.*, Nucl. Phys. **B91**, 266 (1975),

[70] C.E. DeHaven *et al.*, Phys. Rev. Lett. **41**, 669 (1978).

[71] A. Arefiev *et al.*, Nucl. Phys. **B232**, 365 (1984).

[72] B.G. Gibbard *et al.*, Phys. Rev. Lett. **24**, 22 (1970); Nucl. Phys. **B30**, 77 (1971).

[73] F.E. Ringia *et al.*, Phys. Rev. Lett. **28**, 185 (1978).

[74] J.L. Friedes, H. Palevsky, R.L. Stearns, and R. J. Sutter, Phys. Rev. Lett. **15**, 38 (1965).